East European Journal of Physics. **4.** 98-106 (2024)
DOI:10.26565/2312-4334-2024-4-09 ISSN 2312-4334

THERMAL PERFORMANCE OF NANOFLUID FLOW ALONG AN ISOTHERMAL VERTICAL PLATE WITH VELOCITY, THERMAL, AND CONCENTRATION SLIP BOUNDARY CONDITIONS EMPLOYING BUONGIORNO'S REVISED NON-HOMOGENEOUS MODEL

Sujit Mishra, Aditya Kumar Pati, Ashok Misra*, Saroj Kumar Mishra
Centurion University of Technology and Management, Paralakhemundi, Odisha, India
**Corresponding author e-mail: amisra1972@gmail.com*
Received August, 1; 2024; revised October 15, 2024; accepted October 25, 2024

This study examines the natural convection of a steady laminar nanofluid flow past an isothermal vertical plate with slip boundary conditions. A review of existing literature reveals no prior research that has explored the combined effects of thermophoresis, Brownian diffusion, and particle electrification while considering slip boundary conditions in nanofluid flow. Buongiorno's revised four-equation non-homogeneous model, incorporating mechanisms for thermophoresis, Brownian diffusion and particle electrification, is utilized to address this gap. The model employs velocity, thermal, and concentration slip boundary conditions to investigate enhancing the nanofluid's thermal conductivity. The resulting local similar equations are tackled using MATLAB's bvp4c package. The study discusses the influence of key parameters, such as thermophoresis, Brownian motion, and electrification, on temperature, velocity, and concentration distributions, as well as on heat, mass transfer and skin friction coefficients. The findings of the simulation are consistent with previous studies, showing that an improvement in the electrification parameter rises the heat transfer coefficient, while thermophoresis and Brownian motion parameters have the opposite effect. Additionally, mass transfer coefficient values increase with higher Brownian motion and electrification parameters while reducing with the thermophoresis parameter. This physical model has potential applications in heat exchangers using nanofluids and in cooling plate-shaped products during manufacturing processes. The novelty of this study lies in the analysis of Brownian diffusion, thermophoresis, and particle electrification mechanisms in nanofluid flow under slip boundary conditions.
Keywords: *Thermal Conductivity; Nanofluid; Velocity Slip Boundary Condition; Thermal Slip Boundary Condition; Concentration Slip Boundary Condition*
PACS: 44.20.+b, 44.25.+f, 47.10.ad, 47.55.pb, 47.15.Cb

1. INTRODUCTION:

Nanofluids have gained widespread use across numerous industrial applications due to the remarkable chemical and physical properties of nanoscale particles. These nanofluids are sophisticated composite materials composed of solid nanoparticles, typically between 1 and 100 nm in size, dispersed within a liquid medium. The use of nanofluids instead of traditional base fluids to enhance heat transfer rates has garnered significant attention from researchers worldwide, highlighting the distinct advantages of nanofluids over conventional fluids. Nanofluids, which consist of nanoparticles suspended in a base fluid, have been recognized as effective coolants for improving heat transfer performance in various applications. These applications include paper manufacturing, electronic devices, nuclear reactors, power generation, air conditioning systems, domestic refrigerators, and the automotive industry. By leveraging the unique properties of nanofluids, these industries can achieve more efficient thermal management, leading to better performance and energy savings.

The concept of "nanofluids" was first coined by Choi [1], marking a pivotal breakthrough in the study of fluid dynamics at the nanoscale. Subsequent research demonstrated that even a minimal addition of nanoparticles can dramatically improve the thermal conductivity of fluids. Buongiorno [2] further advanced the field by investigating the convective transport phenomena in nanofluids, providing valuable insights into their distinctive flow behaviors. Buongiorno observed that the improvement in the thermal performance of nanofluids is primarily driven by the slip mechanisms of Brownian motion and thermophoresis. Since then, numerous studies, including those by Kuznetsov and Nield [3], Gasmi et al. [4], Ebrahem et al. [5], Kinyanjui et al. [6], Ahmed et al. [7], Biswal et al. [8], Khairul et al. [9], Sobamowo et al. [10], Sobamowo [11], Sobamowo [12], and Aziz and Khan [13] have explored the behavior of natural convection considering different types of nanofluid flow along a vertical plate employing a homogeneous model.

Based on the literature reviewed (Kuznetsov and Nield [3], Mojtabi et al. [14], Abu-Nada et al. [15], Probstein [16], Tyndall [17], Bird et al. [18], Pakravan and Yaghoubi [19]), the slip boundary condition for velocity, temperature, and solute has generally been overlooked. In systems like emulsions, foams, gels, and slurries, the non-homogeneous properties of fluid at solid boundaries often result in "apparent wall slip." This phenomenon happens when the fluid's viscosity near the boundary decreases, leading to the formation of a thin layer with a steep velocity gradient, often described as a "slipping layer." Comprehensive studies on wall slip in shrinking sheets by Makinde et al. [20] reveal that true slip involves a velocity discontinuity at the wall. In contrast, for the other systems discussed, true slip is absent. Instead, "apparent slip" occurs, which is caused by a region with a steeper velocity gradient near the wall. In such cases,

Cite as: S. Mishra, A.K. Pati, A. Misra, S.K. Mishra, East Eur. J. Phys. 4, 98 (2024), https://doi.org/10.26565/2312-4334-2024-4-09

the no-slip condition fails to accurately represent the physical situation, making slip conditions a more suitable choice. Similarly, the no-slip condition is also inadequate for non-Newtonian fluids and nanofluids. During processes like annealing and thinning, the final product's quality is heavily influenced by the heat transfer rate at the continuously stretching surface. Both the stretching kinematics and the concurrent heating or cooling are crucial factors in determining the final product's quality. Therefore, incorporating slip boundary conditions for concentration, temperature, and velocity is essential.

In recent years, several investigations (Pati et al. [21-26], Panda et al. [27], Pattnaik et al. [28]) have explored the electrification of nanoparticles within nanofluid flows under various physical conditions. In all the previously mentioned studies on nanofluid dynamics involving the electrified nanoparticles, the slip boundary conditions have been overlooked.

Based on the past literature, this study aims to investigate the impacts of thermophoresis, Brownian diffusion, and particle electrification on the transfer of heat and mass within the natural convective boundary layer nanofluid flow along an isothermal vertical plate with slip boundary conditions. This study takes into account various boundary conditions, including velocity, thermal, and concentration slip conditions. Buongiorno's revised four-equation non-homogeneous model is employed in the present investigation. This particular approach to modeling the flow of nanofluids concerning heat and mass transport phenomena has not been explored in previous research literature.

2. MATHEMATICAL FORMULATION

An analysis is conducted on a nanofluid's laminar steady boundary layer flow over an isothermal vertical plate. The orientation of the plate is aligned with the vertical axis. It is assumed that both the concentration C_w and temperature T_w of the plate remain invariant. The free stream parameters of C and T defined as C_∞ and T_∞, respectively. The physical representation of the system is illustrated in Fig. 1.

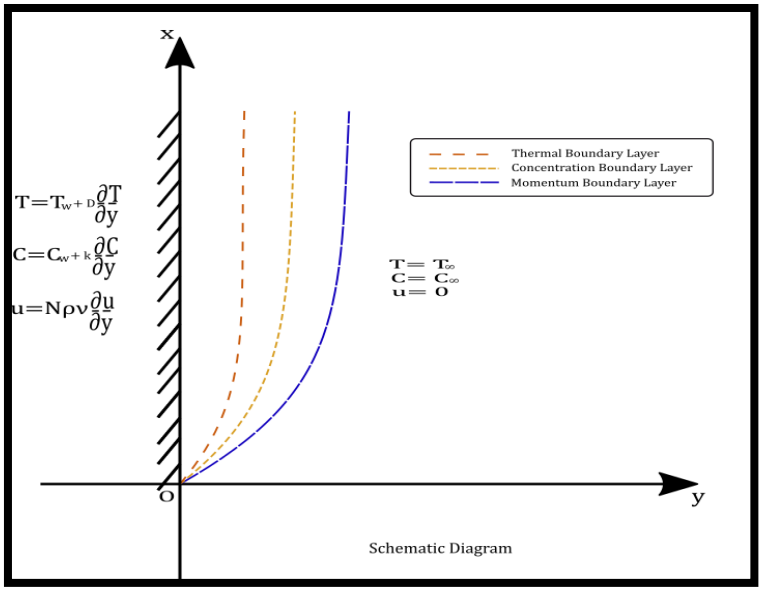

Figure 1. Coordinate system and physical model

Based on the assumptions outlined earlier and applying boundary layer simplifications according to Pati et al. [22], the governing equations for the flow field in a two-dimensional Cartesian coordinate system can be derived and are given as follows.

$$\frac{\partial u}{\partial x}+\frac{\partial v}{\partial y}=0, \tag{1}$$

$$\rho_{nf}\left[u\frac{\partial u}{\partial x}+v\frac{\partial u}{\partial y}\right]=-\frac{\partial p}{\partial x}+\mu_{nf}\left[\frac{\partial^2 u}{\partial y^2}\right]-\rho_{nf}\ g+C\left(\frac{q}{m}\right)E_x, \tag{2}$$

$$\left[u\frac{\partial T}{\partial x}+v\frac{\partial T}{\partial y}\right]=\frac{k_{nf}}{(\rho c)_{nf}}\frac{\partial^2 T}{\partial y^2}+\frac{c_s D_B}{(\rho c)_{nf}}\frac{\partial C}{\partial y}\frac{\partial T}{\partial y}+\frac{\rho_s c_s}{(\rho c)_{nf}}\frac{D_T}{T_\infty}\frac{\partial T}{\partial y}\frac{\partial T}{\partial y}+\left(\frac{q}{m}\right)\frac{c_s C}{F(\rho c)_{nf}}\left(E_x\frac{\partial T}{\partial x}+E_y\frac{\partial T}{\partial y}\right), \tag{3}$$

$$u\frac{\partial C}{\partial x}+v\frac{\partial C}{\partial y}=D_B\frac{\partial^2 C}{\partial y^2}+\frac{\rho_s D_T}{T_\infty}\frac{\partial^2 T}{\partial y^2}+\left(\frac{q}{m}\right)\frac{1}{F}\left[\frac{\partial(CE_x)}{\partial x}+\frac{\partial(CE_y)}{\partial y}\right]. \tag{4}$$

The electric field (E-field) is defined by the following equation.

$$\frac{\partial E_x}{\partial x}+\frac{\partial E_y}{\partial y}=\frac{\rho_s}{\epsilon_0}\frac{q}{m}. \tag{5}$$

According to the Oberbeck-Boussinesq Approximation, the equation of motion in the x-direction, represented by Equation (2), is expressed as follows:

$$\rho_{nf}\left[u\frac{\partial u}{\partial x}+v\frac{\partial u}{\partial y}\right]=\mu_{nf}\left[\frac{\partial^2 u}{\partial y^2}\right]+\beta_{f\infty}\rho_{f_\infty}(T-T_\infty)(1-C_\infty)g-\ (C-C_\infty)\left(\rho_s-\rho_{f\infty}\right)g\ +(C-C_\infty)\left(\frac{q}{m}\right)E_x. \quad (6)$$

The relevant slip boundary conditions for this study are defined by

$$\left.\begin{array}{c} y=0, u=U+N\rho\nu\frac{\partial u}{\partial y}, v=0, T=\mathrm{T}_W+D\frac{\partial T}{\partial y}\ , C=C_W+K\frac{\partial C}{\partial y} \\ y\to\infty\ , u=0\ , v=0\ , T=\ \mathrm{T}_\infty\ \ , C=\ \mathrm{C}_\infty \end{array}\right\}. \quad (7)$$

Based on Soo [29], by disregarding the variation of the electric field in the x-direction, the transverse electric field can be expressed as

$$\frac{\partial \mathrm{E_y}}{\partial y}=\frac{\rho_s}{\epsilon_0}\frac{q}{m}\,.$$

Introducing the stream function and scale analysis of the governing equation (1) are satisfied following Kuznetsov and Nield [3].

$$u=\frac{\partial\psi}{\partial y}, v=-\frac{\partial\psi}{\partial x}, s(\eta)=\frac{C-C_\infty}{C_w-C_\infty},$$

$$\psi\ =\alpha_f(Ra)^{\frac{1}{4}}f(\eta),\ \theta(\eta)=\frac{T-T_\infty}{T_w-T_\infty},$$

where, $\eta=\frac{y}{x}(Ra)^{\frac{1}{4}}$, is the local similarity variable and $Ra_x=\frac{(T_w-T_\infty)(1-C_\infty)\beta_f g x^3}{\nu_f\alpha_f}$, is the local Rayleigh number, we get,

$$u=\frac{\partial\psi}{\partial y}=\frac{\alpha_f(Ra_x)^{\frac{1}{2}}}{x}f',\ v=-\frac{\partial\psi}{\partial x}=-\frac{\alpha_f(Ra_x)^{\frac{1}{4}}}{4x}[3f-\eta f']$$

The equations (2), (3), (4) converted into non-dimensional equations (8), (9), (10) as follows:
Momentum equation:

$$f'''+\frac{\varphi_1}{4Pr}[3ff''-2(f')^2]+\varphi_1\varphi_2\frac{M\,Sc\,N_b}{PrN_F}s+\frac{1}{\varphi_5}(\theta-Nrs\,)=0. \quad (8)$$

Energy equation:

$$\theta''+\frac{3}{4}\frac{1}{\varphi_3\varphi_4}f\theta'+\frac{1}{\varphi_4}\mathrm{Pr}\,N_b s'\theta'+\frac{1}{\varphi_4}\mathrm{Pr}\,N_t(\theta')^2+\frac{1}{\varphi_4}Sc\,N_b\left[\frac{N_F}{N_{Re}}-\frac{1}{4}M\right](s+Nc)\eta\theta'=0. \quad (9)$$

Concentration equation:

$$s''+\frac{3}{4}\frac{Sc}{Pr}fs'+\frac{N_t}{N_b}\theta''-\frac{1}{4}\frac{M\,Sc}{Pr}\eta s'+\frac{N_F Sc}{PrN_{Re}}(\eta s'+s+Nc)\ =0. \quad (10)$$

Similarly, the slip boundary conditions in equation (7) converted into non-dimensional form as follows:

$$\left.\begin{array}{c} \eta=0; f=0;\ f'=Af'', \theta=1+\chi\theta'\ ;\ s=1+\gamma s' \\ \eta\to\infty; f'=0\ ; \theta=0\ ;\ s=0 \end{array}\right\}. \quad (11)$$

where,

$\gamma=K\frac{1}{x}(Ra_x)^{\frac{1}{4}}\ ;\ \chi=D\frac{(Ra_x)^{\frac{1}{4}}}{x}\ ;\ A=N\mu\frac{(Ra_x)^{\frac{1}{4}}}{x}$;

$M=\left(\frac{q}{m}\right)\frac{1}{F\left(\frac{\alpha_f(Ra_x)^{\frac{1}{2}}}{x}\right)}E_x,\ N_F=\frac{\left(\frac{\alpha_f(Ra_x)^{\frac{1}{2}}}{x}\right)}{Fx},\ \frac{1}{N_{Re}}=\left(\frac{q}{m}\right)^2\frac{\rho_s}{\epsilon_0}\frac{x^2}{\left(\frac{\alpha_f(Ra_x)^{\frac{1}{2}}}{x}\right)^2},\ Nr=\frac{(\rho_s-\rho_f)(C_w-C_\infty)}{(1-C_\infty)\rho_f\beta_f(T_w-T_\infty)}$;

$Pr=\frac{\nu_f}{\alpha_f},\ Sc=\frac{\nu_f}{D_B},\ N_b=\frac{(\rho c)_s D_B(C_w-C_\infty)}{(\rho c)_f\nu_f},\ N_t=\frac{(\rho c)_s D_T(T_w-T_\infty)}{(\rho c)_f\nu_f T_\infty},\ N_c=\frac{C_\infty}{(C_w-C_\infty)}$.

This investigation considers a copper water nanofluid which contains 1% of copper nanoparticles. Table-1 provides the thermophysical properties of copper-water nanofluid as outlined by Oztop and Abunada [30], while Table-2 lists the corresponding thermophysical constants.

Table 1. Thermophysical properties

Property	copper	water
$c_p(J/kgK)$	0.385	4.179
$\rho(kg/m^3)$	8933	997.1
$k(W/mK)$	401	0.613

Table 2. Thermophysical constants

φ_1	$(1-C_\infty)^{2.5}\left[C_\infty\frac{\rho_s}{\rho_f}+(1-C_\infty)\right]$
φ_2	$\frac{c_f}{c_s}\frac{1}{\left[C_\infty\frac{\rho_s}{\rho_f}+(1-C_\infty)\right]}$
φ_3	$\frac{1}{C_\infty\tau+(1-C_\infty)}$
φ_4	$\frac{2k_f+k_s-2C_\infty(k_f-k_s)}{2k_f+k_s+C_\infty(k_f-k_s)}$
φ_5	$\frac{1}{(1-C_\infty)^{2.5}}$

The local skin friction C_{fx}, local Sherwood number Sh_x for mass transfer purpose and local Nusselt number Nu_x for heat transfer purpose are given as

$$\frac{(Ra_x)^{\frac{1}{4}}}{Pr}C_{fx}=(f'')_{\eta=0};\quad \frac{1}{(Ra_x)^{\frac{1}{4}}}Nu_x=-(\theta')_{\eta=0};\quad \frac{1}{(Ra_x)^{\frac{1}{4}}}Sh_x=-(s')_{\eta=0},$$

where $(')$ indicates derivative with respect to η and $(f'')_{\eta=0}$, $-(\theta')_{\eta=0}$, and $-(s')_{\eta=0}$ denotes the dimensionless skin friction coefficient, Nusselt number and Sherwood number, respectively.

3. METHOD OF SOLUTION

It has been observed that Pohlhausen-Kuiken-Bejan problems (Bejan [31]) for conventional heat transfer fluids have one non-dimension parameter Pr. However, the non-dimensional equations of the present problem contain nine independent dimensionless parameters, such as Pr, N_b, N_t, N_{Re}, M, Nr, Sc, N_F, Sc. Thus, input selective values are required to solve the problem. Additionally, the processing time for each of these input parameters is quite brief. Since the physical domain extends infinitely while the computational domain is limited, it is essential to select an optimal finite value for η_∞. Since the needed initial value $f''(0), -\theta'(0), -s'(0)$, which are not defined for the present problem**.** Hence, some initial guesses are used at the starting point, as well as some finite values of η_∞, for a specific range of physical parameters. The solution process is iteratively applied with different values of η_∞ until the successive values of $f''(0), -\theta'(0), -s'(0)$ differ by a specified precision. The final η_∞ value obtained is considered the most suitable for that set of parameters. This approach is known as the shooting method.

To address the system of local similarity equations (8)-(10) with the boundary conditions (11) using the shooting method, the MATLAB built-in function bvp4c, which utilizes the collocation technique (as described by Shampine and Kierzenka [32]), is employed to produce numerical results for the specified physical parameters. The variations of the computational values of $(f'')_{\eta=0}$, $-(\theta')_{\eta=0}$ and $-(s')_{\eta=0}$ with different values of M, N_b and N_t, are presented in tabular form. Similarly, the variations of the non-dimensional temperature profile $\theta(\eta)$, non-dimensional velocity profile $f'(\eta)$ and dimensionless concentration distribution of nanoparticles $s(\eta)$ are depicted in Figures 2 to 10.

4. COMPARISON AND VALIDATION

The resultant quantitative data have been contrasted with those computed by Narahari et al. [33], in conjunction with the pertinent values for the particular context of regular fluid outlined in Table 3. The present outcomes exhibit a notable alignment with the prior findings.

Table 3. Comparison of present results with existing literature

Pr	Narahari et al. [33]	Present analysis
1	0.401	0.4010
10	0.459	0.4649
100	0.473	0.4900
1000	0.474	0.4985

5. RESULTS AND DISCUSSION

In this subsection, the impact of M, N_t, and N_b on $f'(\eta)$, $\theta(\eta)$ and $s(\eta)$ against η, illustrated and examined with the help of graphical analysis. Further, the impact of these parameters on $f''(0), -\theta'(0), -s'(0)$ are presented in Tabular form. Additionally, the contour plots are presented to explore the combined effects of M, N_t, and N_b on $f''(0), -\theta'(0), -s'(0)$.

5.1 Influence of electrification parameter M on $f'(\eta)$, $\theta(\eta)$ and $s(\eta)$ with slip boundary conditions

Figures 1 and 2 show that as the parameter M increases, the value of $f'(\eta)$ rises while $\theta(\eta)$ falls throughout the boundary layer. This effect is attributed to the Lorentz force, which results from the electric field acting as an accelerating force that reduces frictional resistance. Consequently, the decrease in frictional resistance leads to a lower temperature in the boundary layer, as no extra thermal energy is produced. Figure 3 depicts the changes in the non-dimensional particle concentration profile $s(\eta)$, illustrating that the concentration decreases with increasing M because the particles are carried away by the fluid moving from the plate. This observed trend suggests that elevated parameter values facilitate particle transport, resulting in a more homogeneous distribution throughout the flow. Figures 2-4 illustrate the variation of $f'(\eta)$, $\theta(\eta)$ and $s(\eta)$ with M while keeping other parameters constant ($A = \chi = \gamma = N_t = N_b = N_F = Nc = Nr = 0.1, Sc = N_{Re} = 2.0$, and $Pr = 6.2$).

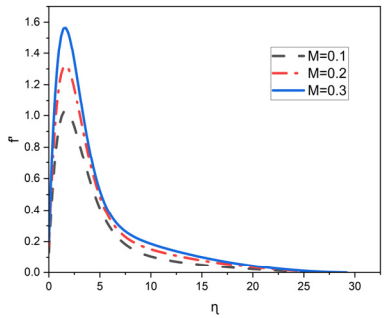

Figure 2. Impact of M on $f'(\eta)$

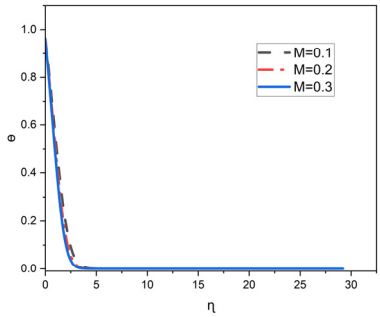

Figure 3. Impact of M on $\theta(\eta)$

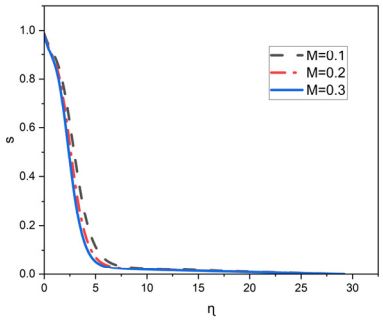

Figure 4. Impact of M on $s(\eta)$

5.2 Influence of thermophoresis parameter N_t on $f'(\eta)$, $\theta(\eta)$ and $s(\eta)$ with slip boundary conditions

Figures 5, 6, and 7 show how the thermophoresis parameter N_t affects on $f'(\eta), \theta(\eta)$, and $s(\eta)$. It is noted that with higher values of N_t, all $f'(\eta)$, $\theta(\eta)$ and $s(\eta)$ profile increases. This is because the increased thermophoresis force causes hot nanoparticles to move faster from the plate region towards the fluid region, thereby raising the dimensionless velocity profiles as well as temperature and concentration profiles. This behaviour is crucial for optimizing the efficiency of thermal systems, as it allows for better heat transfer and enhanced performance in applications such as cooling and energy conversion. Figures 5-7 illustrates the variation of $f'(\eta)$, $\theta(\eta)$ and $s(\eta)$ with N_t while keeping other parameters constant ($A = \chi = \gamma = M = N_b = N_F = Nc = Nr = 0.1, Sc = N_{Re} = 2.0$, and $Pr = 6.2$).

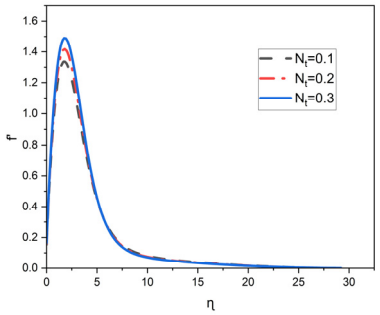

Figure 5. Impact of N_t on $f'(\eta)$

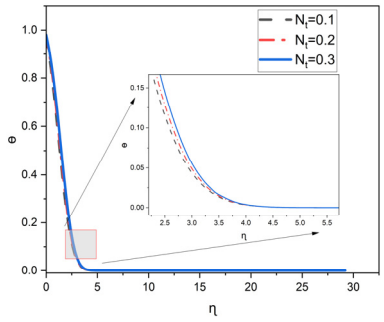

Figure 6. Impact of N_t on $\theta(\eta)$

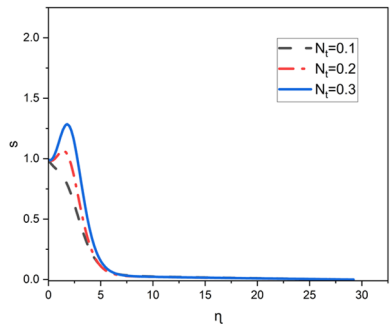

Figure 7. Impact of N_t on $s(\eta)$

5.3. Influence of Brownian motion parameter N_b on $f'(\eta)$, $\theta(\eta)$ and $s(\eta)$ with slip boundary conditions

Brownian motion describes the erratic movement of minute particles suspended in a fluid. This unpredictable motion increases the frequency of collisions between nanoparticles and fluid molecules, leading to the transformation of the molecules' kinetic energy into heat. Smaller particles experience more intense Brownian motion, leading to higher values in N_b. In contrast, larger particles exhibit weaker Brownian motion, resulting in lower values in N_b.

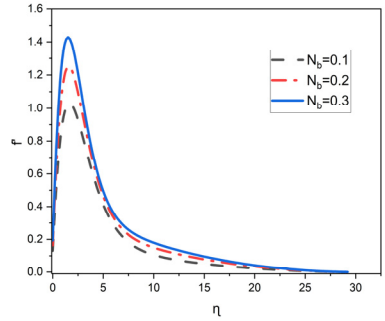

Figure 8. Impact of N_b on $f'(\eta)$

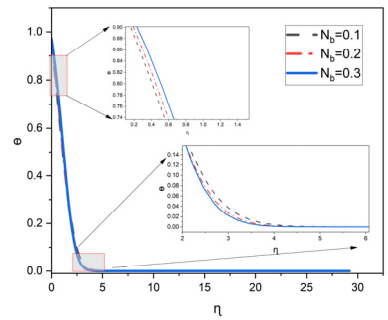

Figure 9. Impact of N_b on $\theta(\eta)$

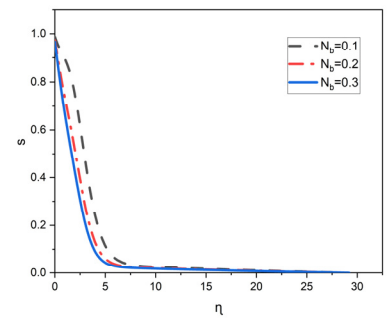

Figure 10. Impact of N_b on $s(\eta)$

Figures 8, 9, and 10 depict the impact of N_b on $f'(\eta), \theta(\eta)$, and $s(\eta)$ profiles. It is observed that the profiles of $f'(\eta)$ show an upward trend, while the $s(\eta)$ shows a downward trend as the values increase for N_b. The profile of $\theta(\eta)$ demonstrates a dual characteristic with the N_b. The temperature distribution increases near the surface of the plate but decreases away from it. As the values in N_b increase, the movement of nanoparticles becomes more pronounced. Consequently, their activity becomes more dynamic, resulting in more frequent collisions within the system. This increased activity promotes a uniform distribution of nanoparticles within the medium, ultimately influencing the system's thermal conductivity and overall performance. Figures 8-10 illustrates the variation of $f'(\eta)$, $\theta(\eta)$ and $s(\eta)$ with N_b while keeping other parameters constant ($A = \chi = \gamma = M = N_t = N_F = Nc = Nr = 0.1, Sc = N_{Re} = 2.0$, and $Pr = 6.2$).

5.4. Influence of M, N_t, and N_b on the non-dimensional skin friction, heat and mass transfer coefficients with slip boundary conditions

Table 4 illustrates the influences of M, N_t, and N_b on $f''(0)$, $-\theta'(0)$ and $-s'(0)$. The values of $f''(0)$ enhances with larger values of all the three parameters M, N_t, and N_b. Values of $-\theta'(0)$ rises as M increases and reduces with higher values of N_t, and N_b. However, $-s'(0)$ improves with M and N_b, but reduces with higher values of N_t.

Table 4. Effects of M, N_t, and N_b on $f''(0)$, $-\theta'(0)$ and $-s'(0)$ when $Sc = N_{Re} = 2.0, Pr = 6.2, A = \chi = \gamma = Nr = Nc = N_F = 0.1$.

M	N_t	N_b	$f''(0)$	$-\theta'(0)$	$-s'(0)$
0.1	0.1	0.1	1.30966	0.37392	0.12734
0.2	0.1	0.1	1.68596	0.41169	0.15141
0.3	0.1	0.1	2.03417	0.44147	0.16622.
0.1	0.1	0.1	1.30966	0.37392	0.12734
0.1	0.2	0.1	1.53577	0.34208	0.07440
0.1	0.3	0.1	1.77814	0.28933	0.07335
0.1	0.1	0.1	1.30966	0.37392	0.12734
0.1	0.1	0.2	1.63950	0.32896	0.27441
0.1	0.1	0.3	1.93596	0.27784	0.33639

5.5. Combined effects of M and N_t on the non-dimensional skin friction, heat and mass transfer coefficients with slip boundary conditions

Combined effects of M and N_t on $f''(0)$, $-\theta'(0)$ and $-s'(0)$ are graphically examined in Figs. 11, 12 and 13, respectively. It is analyzed that all $f''(0)$, $-\theta'(0)$ and $-s'(0)$ are improves with M for different values of N_t. However, only $f''(0)$ increases, whereas both $-\theta'(0)$ and $-s'(0)$ decreases with N_t for varied values of M.

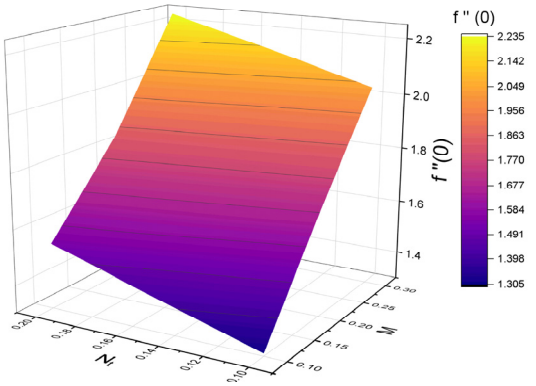

Figure 11. Combined effects of M and N_t on $f''(0)$

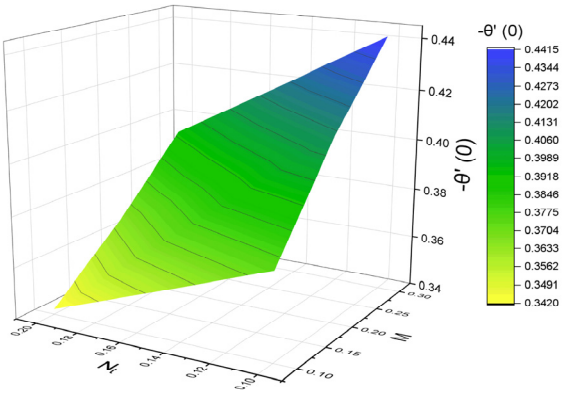

Figure 12. Combined effects of M and N_t on $-\theta'(0)$

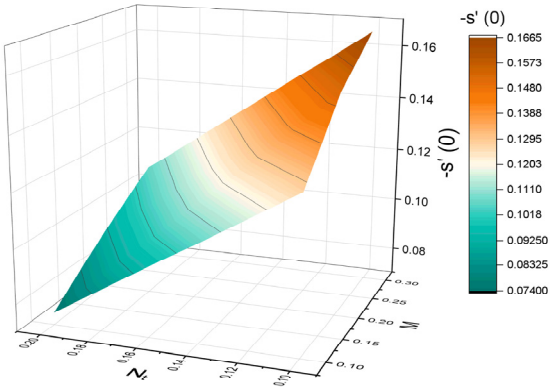

Figure 13. Combined effects of M and N_t on $-s'(0)$

5.6. Combined effects of M and N_b on the non-dimensional skin friction, heat and mass transfer coefficients with slip boundary conditions

Combined effects of M and N_b on $f''(0)$, $-\theta'(0)$ and $-s'(0)$ are graphically explored in Figs. 14, 15 and 16, respectively. It is observed that all the values of $f''(0)$, $-\theta'(0)$ and $-s'(0)$ are enhanced with M for different values of N_b. Additionally, it is noticed that both $f''(0)$ and $-s'(0)$ rises while $-\theta'(0)$ reduces with N_b for varied values of M.

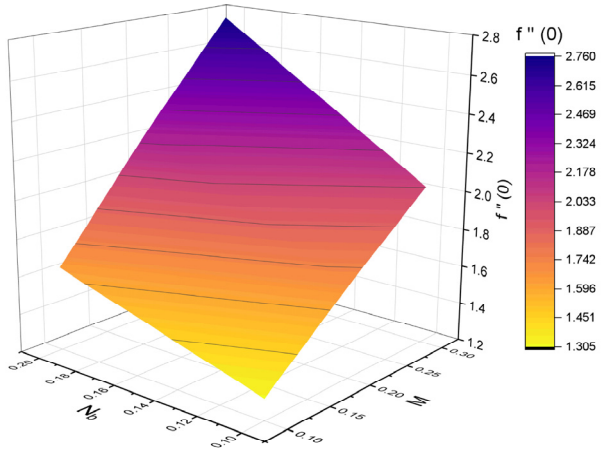

Figure 14. Combined effects of M and N_b on $f''(0)$

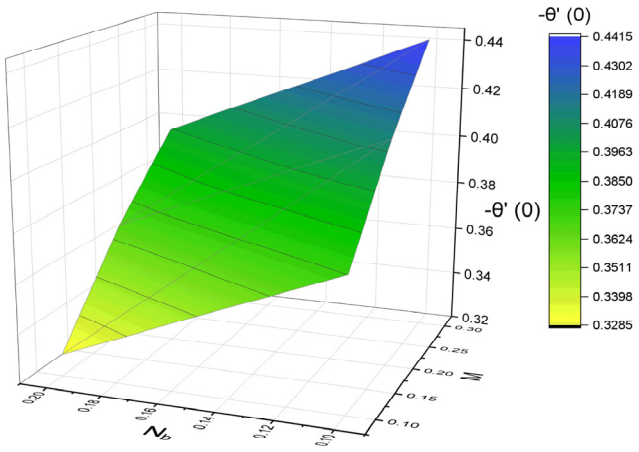

Figure 15. Combined effects of M and N_b on $-\theta'(0)$

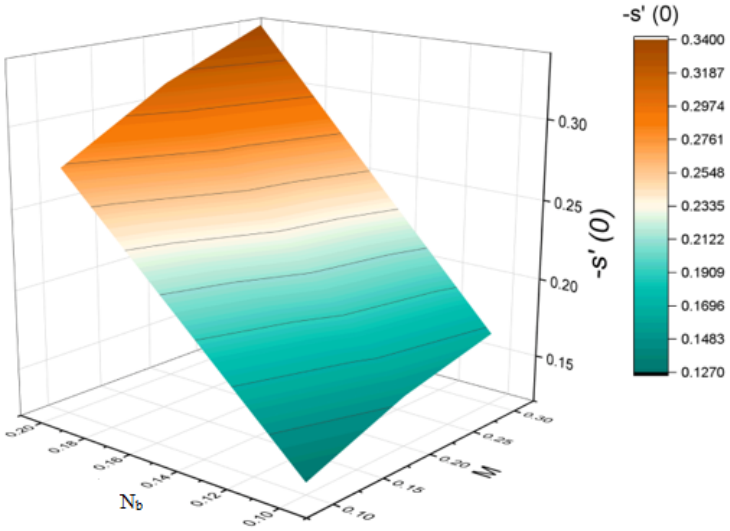

Figure 16. Combined effects of M and N_b on $-s'(0)$

6. CONCLUSIONS

The study successfully examined the steady laminar flow of natural convective Copper-water nanofluid moving along an isothermal vertical plate while considering slip boundary conditions. The outcomes, illustrated and discussed through the figures, reveal a notable impact of control parameters, such as M, N_t and N_b on the non-dimensional temperature, concentration and velocity profiles. In addition, a comprehensive quantitative analysis was conducted on the skin friction, heat transfer, and mass transfer rates of copper-water nanofluid, with a focus on Brownian diffusion, electrification, and thermophoresis mechanisms under slip boundary conditions. This analysis was meticulously presented through detailed tables and contour surface graphs. These visual representations illustrate the impacts of these mechanisms on the reduced skin friction coefficient, heat transfer rate, and mass transfer rate, providing a clear understanding of how each factor influences these parameters. The main findings are as follows:

i. The shooting method implemented in MATLAB's bvp4c effectively addressed the local similarity equations, incorporating velocity, thermal, and concentration slip boundary conditions, ensuring accurate and reliable results.
ii. Dimensionless skin friction coefficient improves with higher values of all the three parameters M, N_t and N_b. Reduced Nusselt number enhances with only M. However, reduced Sherwood number rises with both M and N_b.
iii. An improved understanding of the interplay between electric fields, thermophoresis, and Brownian motion using copper water nanofluids can lead to developing more efficient cooling systems for compact and smart heat exchanger devices.

The findings of this study provide valuable insights into the behavior of electrified nanofluids with velocity, thermal, and concentration slip boundary conditions that can be applied to enhance thermal management in various engineering applications.

Nomenclature

A	Velocity slip parameter	N_t	Thermophoresis parameter
χ	Temperature slip parameter	Nr	Buoyancy ratio
γ	Concentration slip parameter	Nc	Concentration ratio
N	Velocity slip factor	N_F	Momentum transfer number
D	Thermal slip factor	N_{Re}	Electric Reynolds number
K	Concentration slip factor	Sc	Schmidt number
U, C, T	Local velocity, concentration & temperature	β_f	Volumetric thermal expansion coefficient
C_∞, T_∞	Free stream concentration & temperature	F	Momentum transfer time constant between the fluid and nanoparticles
C_w, T_w	Wall Surface concentration & temperature	ϵ_0	Permittivity
u, v	Velocity Component in direction x, y	ρ_s	Density of solid particles
E_x, E_y	Electric Intensity Component in direction x, y	ρ_f	Density of base fluid
g	Gravitational acceleration	ρ_{nf}	Density of nanofluid
D_T	Thermophoretic diffusion coefficient	μ_f	Viscosity of base fluid
D_B	Brownian diffusion coefficient	μ_{nf}	Viscosity of nanofluid
m	Mass of the nanoparticle	k_s	Thermal conductivity of solid particles
q	Charge of the nanoparticle	k_f	Thermal conductivity of base fluid
p	Pressure	k_{nf}	Thermal conductivity of nanofluid
Pr	Prandtl number	c_s	Specific heat capacity of solid particles
M	Electrification parameter	c_f	Specific heat capacity of base fluid
N_b	Brownian motion parameter	c_{nf}	Specific heat capacity of nanofluid

ORCID

Sujit Mishra, https://orcid.org/0000-0003-0106-7234; **Aditya Kumar Pati,** https://orcid.org/0000-0003-0966-5773
Ashok Misra, https://orcid.org/0000-0002-1148-1378; **Saroj Kumar Mishra,** https://orcid.org/0009-0005-2217-2764

REFERENCES

[1] S.U.S. Choi, Z.G. Zhang, W. Yu, F.E. Lockwood, and E.A. Grulke, "Anomalously thermal conductivity enhancement in nanotube suspensions," Applied Physics Letters, **79**, 2252-2254 (2001). https://doi.org/10.1063/1.1408272
[2] J. Buongiorno, "Convective transport in nanofluids," ASME J. Heat Transf. **128**, 240-250 (2006). https://doi.org/10.1115/1.2150834
[3] A.V. Kuznetsov, and D.A. Nield, "Natural convective boundary-layer flow of a nanofluid past a vertical plate," Int. J. Thermal Sci. **49**, 243-247 (2010). https://doi.org/10.1016/j.ijthermalsci.2009.07.015
[4] H. Gasmi, U. Khan, A. Zaib, A. Ishak, S.M. Eldin, and Z. Raizah, "Analysis of Mixed Convection on Two-Phase Nanofluid Flow Past a Vertical Plate in Brinkman-Extended Darcy Porous Medium with Nield Conditions," Mathematics, **10**(20), 3918 (2022). https://doi.org/10.3390/math10203918
[5] E.A. Algehyne, M. Areshi, A. Saeed, M. Bilal, W. Kumam, and P. Kumam, "Numerical simulation of bioconvective Darcy Forchhemier nanofluid flow with energy transition over a permeable vertical plate," Scientific Reports, **12**, 3228 (2022). https://doi.org/10.1038/s41598-022-07254-9
[6] J.K. Kigio, M.W. Nduku, and O.A. Samuel, "Analysis of Volume Fraction and Convective Heat Transfer on MHD Casson Nanofluid over a Vertical Plate," Fluid Mechanics, **7**(1), (2021). https://doi.org/10.11648/J.FM.20210701.11
[7] N. Ahmed, N.A. Shah, B. Ahmad, S.I. Shah, S. Ulhaq, M.R. Gorji, "Transient MHD Convective Flow of Fractional Nanofluid between Vertical Plates," Applied and Computational Mechanics, **5**(4), 592-602 (2019). https://doi.org/10.22055/JACM.2018.26947.1364
[8] U. Biswal, S. Chakraverty, and B.K. Ojha, "Natural convection of nanofluid flow between two vertical flat plates with imprecise parameter," Coupled systems mechanics, **9**(3), 219-235 (2020). https://doi.org/10.12989/CSM.2020.9.3.219
[9] M.K.A. Mohamed, H.R. Ong, M.Z. Salleh, and B. Widodo, "Mixed convection boundary layer flow of engine oil nanofluid on a vertical flat plate with viscous dissipation," Journal of Automotive Technology, **1**(1), 29–38 (2019). https://www.journal.dhuautomotive.edu.my/autojournal/article/view/7/6
[10] G. Sobamowo, and A.A. Yinusa, "Insight into the Boundary Layer Flows of Free Convection and Heat Transfer of Nanofluids over a Vertical Plate using Multi-Step Differential Transformation Method," Iranian Journal of Mechanical Engineering Transactions of the ISME, (2019).
[11] G. Sobamowo, "Free Convection Flow and Heat Transfer of Nanofluids of Different Shapes of Nano-Sized Particles over a Vertical Plate at Low and High Prandtl Numbers," Journal of Applied and Computational Mechanics, **5**(1), 13-39 (2019). https://doi.org/10.22055/JACM.2018.24529.1196
[12] G. Sobamowo, "Combined Effects of Thermal Radiation and Nanoparticles on Free Convection Flow and Heat Transfer of Casson Fluid over a Vertical Plate," International Journal of Chemical Engineering, (2018). https://doi.org/10.1155/2018/7305973
[13] A. Aziz, and W.A. Khan, "Natural convective boundary layer flow of a nanofluid past a convectively heated vertical plate," International Journal of Thermal Sciences, **52**, 83-90 (2012). https://doi.org/10.1016/j.ijthermalsci.2011.10.001
[14] Mojtabi, M.C. Charrier-Mojtabi, "Double-diffusive convection in porous media," in: *Handbook of Porous Media*, edited by K. Vafai, (Dekker, New York, 2000).

[15] E. Abu-Nada, Z. Masoud, H.F. Oztop, and A. Campo, "Effect of nanofluid variable properties on natural convection in enclosures," Int. J. Therm. Sci. **49**, 479-491 (2010). https://doi.org/10.1016/j.ijthermalsci.2009.09.002
[16] R.F. Probstein, *Physicochemical Hydrodynamics*, second ed., (Wiley Interscience, Hoboken, New Jersey, 2003)
[17] J. Tyndall, "On dust and disease," Proc. R. Inst. **6**, 1-14 (1870).
[18] R.B. Bird, W.E. Stewart, and E.N. Lightfoot, *Transport Phenomena*, second ed. (Wiley, New York, 1960).
[19] H.A. Pakravan, and M. Yaghoubi, "Combined thermophoresis, Brownian motion and Dufour effects on natural convection of nanofluids," Int. J. Therm. Sci. **50**, 394-402 (2011). https://doi.org/10.1016/j.ijthermalsci.2010.03.007
[20] O.D. Makinde, W.A. Khan, Z.H. Khan, "Buoyancy effects on MHD stagnation point flow and heat transfer of a nanofluid past a convectively heated stretching/shrinking sheet," International Journal of Heat and Mass Transfer, **62**, 526-533 (2013). http://dx.doi.org/10.1016%2Fj.ijheatmasstransfer.2013.03.049
[21] A.K. Pati, A. Misra, and S.K. Mishra, "Effect of electrification of nanoparticles on heat and mass transfer in boundary layer flow of a copper water nanofluid over a stretching cylinder with viscous dissipation," JP journal of heat and mass transfer, **17**(1), 97-117 (2019). http://dx.doi.org/10.17654/HM017010097
[22] A.K. Pati, A. Misra, S.K. Mishra, S. Mishra, R. Sahu, and S. Panda, "Computational modelling of heat and mass transfer optimization in copper water nanofluid flow with nanoparticle ionization," JP Journal of Heat and Mass Transfer, **31**, 1-18 (2023). https://doi.org/10.17654/0973576323001
[23] A.K. Pati, A. Misra, and S.K. Mishra, "Heat and mass transfer analysis on natural convective boundary layer flow of a Cu-water nanofluid past a vertical Flat plate with electrification of nanoparticles," Advances and Applications in Fluid Mechanics, **23**(1), 1-15 (2019). http://dx.doi.org/10.17654/FM023010001
[24] A.K. Pati, S. Mishra, A. Misra, and S.K. Mishra, "Heat and Mass Transport Aspects of Nanofluid Flow towards a Vertical Flat Surface influenced by Electrified Nanoparticles and Electric Reynolds Number," East European Journal of Physics, (2), 234-241 (2024). https://doi.org/10.26565/2312-4334-2024-2-22
[25] A.K. Pati, A. Misra, and S.K. Mishra, "Effect of electrification of nanoparticles on natural convective boundary layer flow and heat transfer of a Cu-Water nanofluid past a vertical flat plate," International Journal of Engineering, Science and Mathematics, **6**(8), 1254-1264 (2017). https://www.ijmra.us/project%20doc/2017/IJESM_DECEMBER2017_Special_Issue/4553_pdf.pdf
[26] A.K. Pati, A. Misra, and S.K. Mishra, "Modeling electrification of nanoparticles in free convective nanofluid flow," TEST Engineering and Management, (83), 17663-17669 (2020). http://testmagzine.biz/index.php/testmagzine/article/view/6854/5299
[27] S. Panda, A. Misra, S.K. Mishra, A.K. Pati, and K.K. Pradhan, "Flow and Heat Transfer Analysis of H2O-Al2O3 Nanofluid Over a Stretching Surface with Electrified Nanoparticles and Viscous Dissipation," Advances in Dynamical Systems and Applications, **16**(2), 1533-1545 (2021).
[28] R. Pattnaik, A. Misra, S.K. Mishra, K. Kumar, S.P. Pradhan, and A.K. Pati, "Thermal Performance Analysis of Nanofluid Past an Exponentially Stretching Surface Due to the Electrification Effect of Nanoparticles," International Journal of Difference Equations (IJDE), **16**(2), 189-203 (2021). https://www.ripublication.com/ijde21/v16n2p02.pdf
[29] S.L. Soo, "Effect of electrification on the dynamics of a particulate system," Industrial and Engineering Chemistry Fundamentals **3**, 75-80 (1964). https://doi.org/10.1021/i160009a013
[30] H.F. Oztop, and E. Abu-Nada, "Numerical study of natural convection in partially heated rectangular enclosures filled with nanofluids," International Journal of Heat Fluid Flow, **29**, 1326-1336 (2008). https://doi.org/10.1016/j.ijheatfluidflow.2008.04.009
[31] Adrian Bejan, *Convection Heat Transfer*, (John Wiley and Sons, 2013).
[32] J. Kierzenka, and L.F. Shampine, "A BVP Solver based on residual control and the MATLAB PSE," ACM Trans. Math. Softw. **27**(3), 299–316 (2001).
[33] M. Narahari, S. Akilu and A. Jaafar, *Free convection flow of a nanofluid past an isothermal inclined plate*, in: *Applied Mechanics and Materials*, vol. 390, (Trans Tech Publications Ltd. 2013).

ТЕПЛОВІ ХАРАКТЕРИСТИКИ ПОТОКУ НАНОРІДИНИ ВЗДОВЖ ІЗОТЕРМІЧНОЇ ВЕРТИКАЛЬНОЇ ПЛАСТИНИ З ГРАНИЧНИМИ УМОВАМИ ШВИДКОСТІ, ТЕПЛОВОГО ТА КОНЦЕНТРАЦІЙНОГО КОВЗАННЯ ЗА ВИКОРИСТАННЯ ПЕРЕГЛЯНУТОЇ НЕОДНОРІДНОЇ МОДЕЛІ БУОНДЖОРНО

Суджит Мішра, Адітя Кумар Паті, Ашок Міспа, Сародж Кумар Мішра
Університет технології та менеджменту Центуріон, Паралахемунді, Одіша, Індія

У цій роботі досліджується природна конвекція постійного ламінарного потоку нанофлюїду повз ізотермічну вертикальну пластину з граничними умовами ковзання. Огляд існуючої літератури не виявив жодних попередніх досліджень, які б досліджували комбіновані ефекти термофорезу, броунівської дифузії та електризації частинок при розгляді граничних умов ковзання в потоці нанорідин. Переглянута неоднорідна модель із чотирьох рівнянь Буонджорно, що включає механізми термофорезу, броунівської дифузії та електризації частинок, використовується для усунення цієї прогалини. Модель використовує граничні умови швидкості, тепла та концентраційного ковзання для дослідження підвищення теплопровідності нанофлюїду. Отримані локальні аналогічні рівняння обробляються за допомогою пакета bvp4c MATLAB. У дослідженні обговорюється вплив ключових параметрів, таких як термофорез, броунівський рух і електризація, на температуру, швидкість і розподіл концентрації, а також на тепло-, масообмін і коефіцієнти тертя шкіри. Результати моделювання узгоджуються з попередніми дослідженнями, показуючи, що покращення параметра електризації підвищує коефіцієнт теплопередачі, тоді як параметри термофорезу та броунівського руху мають протилежний ефект. Крім того, значення коефіцієнта масопередачі збільшуються з вищими параметрами броунівського руху та електризації, одночасно зменшуючись із параметром термофорезу. Ця фізична модель має потенційне застосування в теплообмінниках з використанням нанофлюїдів і в охолодженні пластинчастих продуктів під час виробничих процесів. Новизна цього дослідження полягає в аналізі механізмів броунівської дифузії, термофорезу та електризації частинок у потоці нанофлюїдів за граничних умов ковзання.

Ключові слова: *теплопровідність; нанофлюїд; гранична умова швидкісного ковзання; граничний стан термічного ковзання; гранична умова концентраційного ковзання*